INVERSE KINEMATICS AND DYNAMICS ANALYSIS OF A THREE LEGGED PARALLEL MECHANISM ACTUATED BY AGVs

Georgios Rekleitis and Meyer Nahon
McGill University
Department of Mechanical Engineering
817 Sherbrooke Street West
Montreal, Quebec H3A 2K6
CANADA

Subir K. Saha
Indian Institute of Technology Delhi
Department of Mechanical Engineering
Hauz Khas, New Delhi 110 016
INDIA

ABSTRACT

In this paper, the inverse kinematics and inverse dynamics analysis of a parallel mechanism is presented. The mechanism consists of three fixed-length legs each supported by a three-wheeled mobile robot. The three legs support a platform, which acts as the end-effector of the mechanism. Two different designs are evaluated: one with ball joints at the top ends of the legs and revolute joints at the lower ends and one with the opposite configuration. Inverse kinematics and dynamics analysis is also performed for the three actuators (mobile robots). Simulations are shown in order to compare the performance of the two configurations. Of the two designs, the one with ball joints at the lower end of the legs is found to perform better.

RESUME

Cet article traite l'analyse de la cinématique inverse et dynamique inverse d'un mécanisme parallèle à trois pattes. Chaque patte est soutenue par un véhicule robotique à trois roues. Les trois pattes, ensembles, soutiennent une plateforme commune. Deux différentes conceptions sont evaluées: une avec des articulations sphériques au extrémités supérieures des pattes et des articulations rotoïdes aux extrémités inférieures, et l'autre avec une configuration contraire. L'analyse cinématique inverse et dynamique inverse est aussi effectuée pour les véhicules robotiques. A l'aide de simulations, nous démontrons les différences de performances entre les deux configurations, et que le mécanisme avec les articulations sphériques au extrémités inférieures des pattes est préférable.

1. INTRODUCTION

Robotic mechanisms can be divided in two classes: Serial mechanisms and parallel mechanisms. Of these, serial mechanisms are the most commonly used. Nevertheless, parallel mechanisms have a number of advantages over serial ones, which have led to an increasing interest in them. The main advantages of parallel mechanisms are: (a) higher payload-to-weight ratio, (b) higher accuracy, and (c) simpler solution of the inverse kinematics problem.

On the other hand, parallel mechanisms have some disadvantages, most importantly: (a) smaller workspace, (b) more frequent occurrence of singularities within the workspace, and (c) more difficult solutions of the direct kinematics problem.

A parallel mechanism introduced by V. E. Gough in 1956 [1] (which also appears in the commentary of a paper by D. Stewart in 1965 [2], thus acquiring the name "Stewart-Platform") is one of the best-known six degree-of-freedom (dof) parallel mechanisms. This mechanism has been studied extensively since and several similar configurations have emerged as a result [3,4,5].

A different six-dof parallel mechanism was studied by Ben-Horin et al. [6,7] and by Tsai and Tahmasebi [8,9,10]. Instead of having six legs of variable length whose lower ends are anchored to the ground, this device has three legs of fixed length, actuated by three two-dof planar motors. This configuration allows a larger work-volume, thus alleviating one of the drawbacks of parallel mechanisms.

In this paper, a similar parallel mechanism is presented and analyzed. Here, the planar actuators are replaced by three wheeled mobile robots, or "Automatic Guided Vehicles" (AGVs). Thus, our system consists of a platform with an equilateral triangle profile, which is supported by three fixed-length legs, each of which is supported by an AGV (Figure 1). Two different configurations are tested: one with ball joints at the upper ends of the legs and revolute joints at the lower ends and one with the opposite joint configuration. The intended application for this mechanism is as a portable flight simulator motion base. In this application, the reduced accuracy resulting from the use of AGVs as actuators is less important than the advantage of portability which they allow.
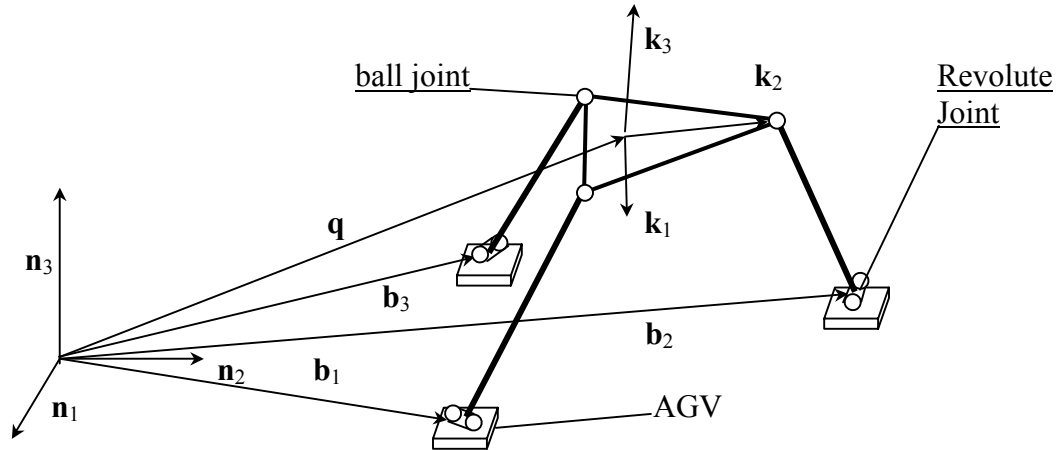

Figure 1. 3-D Representation of the System.

2. INVERSE KINEMATICS ANALYSIS

In Figure 2, a top view of the system is shown. In this figure, two coordinate frames are used: the inertial frame ($\mathbf{n}_1$, $\mathbf{n}_2$, $\mathbf{n}_3$) and the platform frame ($\mathbf{k}_1$, $\mathbf{k}_2$, $\mathbf{k}_3$). The inertial frame's $\mathbf{n}_1$-$\mathbf{n}_2$ plane is parallel to the plane on which the AGVs are moving and at the level of the centers of the lower joints. The platform frame is attached to the platform as shown in Figure 2 and has its origin at the mass center of the platform. As a result, vector $\mathbf{k}_3$ is normal to the platform. Vector $\mathbf{q}$ is the position vector of the origin of the platform frame, while vector $\mathbf{b}_i$ is the position vector of a reference point on the ith AGV, both expressed in the inertial frame. Vector $\mathbf{r}_i$ is the vector along the ith leg (from bottom to top), with a magnitude equal to the leg length. Vector $\mathbf{p}^i_{abs}$ is the vector from the mass center of the platform to the top of the ith leg and is also expressed in the inertial frame.

Two different configurations of joints are studied: ball joints at the upper end of the legs and revolute joints at the lower end and the reverse case. In both configurations, the AGV platform has a fixed orientation.

2.1 Ball joints at the upper end of legs

In Figure 3 another coordinate frame is introduced. In this figure, the lower part of the ith leg is shown, along with the corresponding Leg Frame ($\mathbf{x}^i_{leg}$, $\mathbf{y}^i_{leg}$, $\mathbf{z}^i_{leg}$). Note that the $\mathbf{z}^i_{leg}$ axis is along the leg and that $\mathbf{x}^i_{leg}$ axis is along the axis of the revolute and always in the $\mathbf{n}_1$-$\mathbf{n}_2$ plane. Angle β_i is the inclination angle of the ith leg. Each leg moves in a plane that is perpendicular to the $\mathbf{n}_1$-$\mathbf{n}_2$ plane. The orientation of this plane with respect to $\mathbf{n}_2$ is constant at an angle α_i. This is so because the orientation of the platform of each AGV is kept constant and so is the orientation of the revolute joints that connect the AGVs with the legs. The angles α_i are positive clockwise.
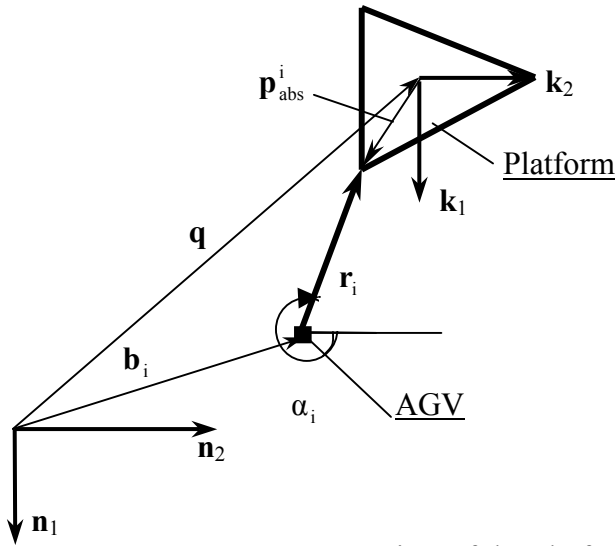

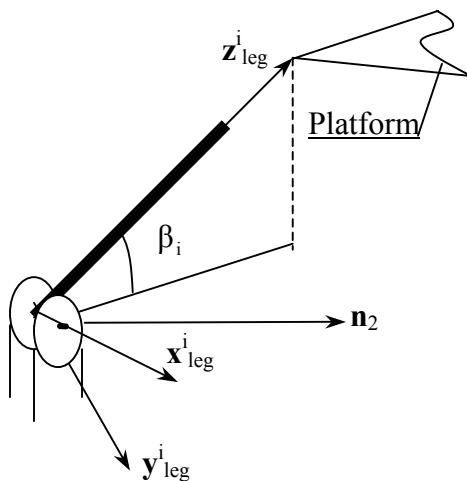**Figure 2.** Top view of the platform (only one leg shown).

Figure 3. Revolute joint at lower end of the leg.

2.1.1 Position Inverse Kinematics

The position inverse kinematics for the platform requires that we find the components of $\mathbf{b}_i$, given the position and orientation of the platform. The approach to solve this problem used here is based on that shown in [7]. From Figure 2 it is apparent that:

$$\mathbf{b}_i = \mathbf{q} + \mathbf{p}^i_{abs} - \mathbf{r}_i \tag{1}$$

From Figure 3, we find:

$$\mathbf{r}_i = \begin{bmatrix} l_i \cos(\beta_i)\sin(\alpha_i) \\ l_i \cos(\beta_i)\cos(\alpha_i) \\ l_i \sin(\beta_i) \end{bmatrix} \tag{2}$$

where l_i is the length of the ith leg. Equations (1) and (2) can be rewritten as a system of equations:

$$b_{i,x} = q_x + p^i_{abs,x} - l_i \cos(\beta_i)\sin(\alpha_i) \tag{3a}$$

$$b_{i,y} = q_y + p^i_{abs,y} - l_i \cos(\beta_i)\cos(\alpha_i) \tag{3b}$$

$$b_{i,z} = q_z + p^i_{abs,z} - l_i \sin(\beta_i) \tag{3c}$$

Since the $\mathbf{n}_1$-$\mathbf{n}_2$ plane is parallel to the plane on which the AGVs move and it passes through the centers of the revolute joints, $b_{i,z} = 0$. From equation (3c), we obtain β_i:

$$\beta_i = \sin^{-1}\left(\frac{q_z + p^i_{abs,z}}{l_i}\right) \tag{4}$$

With the help of equation (4), equations (3a) and (3b) provide the remaining components of $\mathbf{b}_i$ for the three AGVs.

2.1.2 Velocity Inverse Kinematics

From Figures 2 and 3 we can see that, if $\boldsymbol{\omega}_p$ is the platform angular velocity vector, the velocity of the upper end of each leg, at the center of the ball joint ($\mathbf{v}_i$), can be given by two distinct expressions:

$$\mathbf{v}_i = \dot{\mathbf{q}} + \boldsymbol{\omega}_p \times \mathbf{p}^i_{abs} \tag{5a}$$

$$\mathbf{v}_i = \dot{\mathbf{b}}_i + \boldsymbol{\omega}^i_{leg} \times l_i \mathbf{z}^i_{leg} \tag{5b}$$

which leads to:

$$\dot{\mathbf{q}} + \boldsymbol{\omega}_p \times \mathbf{p}^i_{abs} = \dot{\mathbf{b}}_i + \boldsymbol{\omega}^i_{leg} \times l_i \mathbf{z}^i_{leg} \tag{6}$$

where the superscripts and subscripts i stand for the ith leg and l_i is the length of the ith leg. Note that vector $\dot{\mathbf{b}}_i$ is equal to $\dot{\mathbf{b}}_i = \begin{bmatrix} \dot{x}_i & \dot{y}_i & 0 \end{bmatrix}^T$, where x_i and y_i are the position coordinates of the ith AGV in the inertial frame. Vector $\boldsymbol{\omega}^i_{leg}$ is the vector of the angular velocity of the ith leg. Furthermore, if vector $\boldsymbol{\beta}$ is defined as the vector of magnitude β_i and direction $\mathbf{x}^i_{leg}$ (which is also the direction of $\boldsymbol{\omega}^i_{leg}$), then we have:

$$\boldsymbol{\beta}_i = \beta_i \begin{bmatrix} \cos(\alpha_i) \\ \sin(\alpha_i) \\ 0 \end{bmatrix} \tag{7}$$

Then, since angles α_i are constant, differentiating both sides of equation (7), leads to:

$$\dot{\boldsymbol{\beta}}_i = \dot{\beta}_i \begin{bmatrix} \cos(\alpha_i) \\ \sin(\alpha_i) \\ 0 \end{bmatrix} = \dot{\beta}_i \mathbf{x}_{leg}^i \tag{8}$$

Finally, since the leg undergoes only a rotation due to $\dot{\boldsymbol{\beta}}_i$, its angular velocity is:

$$\boldsymbol{\omega}_{leg}^i = \dot{\boldsymbol{\beta}}_i = \dot{\beta}_i \mathbf{x}_{leg}^i \tag{9}$$

So, equation (6) becomes:

$$\dot{\mathbf{q}} + \boldsymbol{\omega}_p \times \mathbf{p}_{abs}^i = \dot{\mathbf{b}}_i + \dot{\beta}_i \mathbf{x}_{leg}^i \times l_i \mathbf{z}_{leg}^i = \dot{\mathbf{b}}_i + \dot{\beta}_i l_i \left(\mathbf{x}_{leg}^i \times \mathbf{z}_{leg}^i \right) \tag{10}$$

Pre-multiplying both sides of equation (10) by $\left(\mathbf{x}_{leg}^i \times \mathbf{z}_{leg}^i \right)^T$, we obtain:

$$\left(\mathbf{x}_{leg}^i \times \mathbf{z}_{leg}^i \right)^T \left[\dot{\mathbf{q}} + \boldsymbol{\omega}_p \times \mathbf{p}_{abs}^i \right] = \left(\mathbf{x}_{leg}^i \times \mathbf{z}_{leg}^i \right)^T \dot{\mathbf{b}}_i + \left(\mathbf{x}_{leg}^i \times \mathbf{z}_{leg}^i \right)^T \left(\mathbf{x}_{leg}^i \times \mathbf{z}_{leg}^i \right) \dot{\beta}_i l_i$$

With $\mathbf{y}_{leg}^i = -\mathbf{x}_{leg}^i \times \mathbf{z}_{leg}^i$ and solving for $\dot{\beta}_i$ and substituting in equation (10), we obtain:

$$\dot{\mathbf{q}} + \boldsymbol{\omega}_p \times \mathbf{p}_{abs}^i = \dot{\mathbf{b}}_i - \mathbf{y}_{leg}^{i\,T} \left[\dot{\mathbf{q}} + \boldsymbol{\omega}_p \times \mathbf{p}_{abs}^i - \dot{\mathbf{b}}_i \right] \left(-\mathbf{y}_{leg}^i \right) \tag{11}$$

Using the identity $\mathbf{u}_1^T \mathbf{u}_2 \mathbf{u}_1 = \mathbf{u}_1 \mathbf{u}_1^T \mathbf{u}_2$ we can rewrite equation (11) as:

$$\left[\mathbf{I}_{3x3} - \mathbf{y}_{leg}^i \mathbf{y}_{leg}^{i\,T} \right] \dot{\mathbf{b}}_i = \left[\mathbf{I}_{3x3} - \mathbf{y}_{leg}^i \mathbf{y}_{leg}^{i\,T} \right] \left[\dot{\mathbf{q}} + \boldsymbol{\omega}_p \times \mathbf{p}_{abs}^i \right] \tag{12}$$

Equation (12) can be written as $\mathbf{A} \dot{\mathbf{b}}_i = \mathbf{c}$ and solved for $\dot{\mathbf{b}}_i$.

2.1.3 Acceleration Inverse Kinematics

In equation (1), vectors $\mathbf{p}_{abs}^i$ are expressed in the inertial frame. If we express them in the platform frame ($\mathbf{p}^i$), then they are constant vectors. In that case, $\mathbf{p}_{abs}^i$ in equation (1) is replaced by $\mathbf{R}\mathbf{p}^i$ where $\mathbf{R}$ is the rotation matrix that transforms vectors from the platform frame to the inertial frame. By differentiating equation (6), we obtain:

$$\ddot{\mathbf{q}} + \dot{\boldsymbol{\omega}}_p \times \mathbf{R}\mathbf{p}^i + \boldsymbol{\omega}_p \times \left(\boldsymbol{\omega}_p \times \mathbf{R}\mathbf{p}^i \right) = \ddot{\mathbf{b}}_i + \ddot{\beta}_i \times l_i \mathbf{z}_{leg}^i + \dot{\beta}_i \times l_i \dot{\mathbf{z}}_{leg}^i = $$
$$\ddot{\mathbf{b}}_i + \ddot{\beta}_i l_i \left(\mathbf{x}_{leg}^i \times \mathbf{z}_{leg}^i \right) + \dot{\beta}_i \times l_i \dot{\mathbf{z}}_{leg}^i \tag{13}$$

Using a similar approach to that used in the velocity inverse kinematics analysis, $\ddot{\mathbf{b}}_i$ can be obtained.

2.2 Ball joint at the lower end of the legs

In this configuration, the planes in which the legs are moving are perpendicular to the plane of the moving platform and angles α_i are no longer constant. The orientations of each plane are at an angle α_i^p with respect to $\mathbf{k}_2$, as shown in Figure 4.

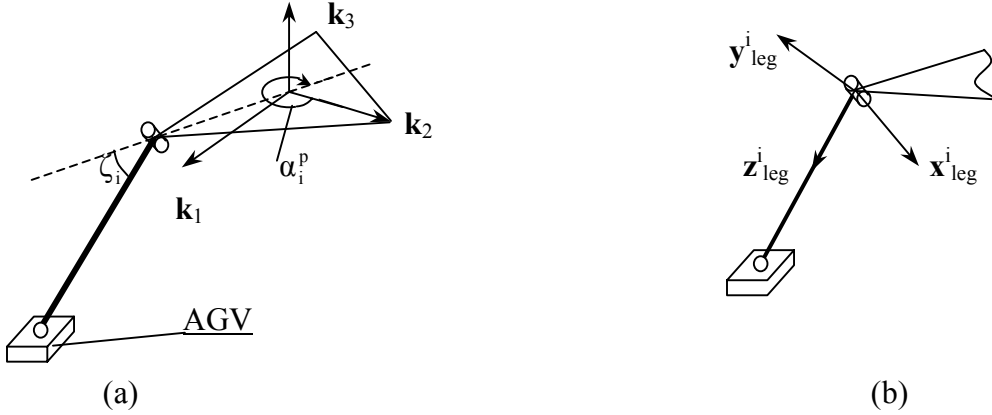(a)   (b)

Figure 4. System with ball joint at the lower end of the leg and new leg frame.

2.2.1 Position Inverse Kinematics

A new leg coordinate frame is introduced in Figure 4. From that Figure, it is apparent that the lower end of each leg is moving on a circle, in the leg frame, of radius l_i. So we have:

$$z_{leg}^i = -l_i \tag{14}$$

$$x_{leg}^i = y_{leg}^i = 0 \tag{15}$$

where $x^i{}_{leg}$, $y^i{}_{leg}$ and $z^i{}_{leg}$ are the components of $\mathbf{r}_i$ expressed in the leg frame (Figure 4b). From Figure 2 it is apparent that:

$$\begin{bmatrix} x_{leg}^i \\ y_{leg}^i \\ z_{leg}^i \end{bmatrix} = \mathbf{R}_i^{tot} \left\{ \begin{bmatrix} b_{i,x} \\ b_{i,y} \\ b_{i,z} \end{bmatrix} - \left(\mathbf{q} + \mathbf{p}_{abs}^i \right) \right\} \tag{16}$$

where $\mathbf{R}_i^{tot}$ is the Rotation matrix that transforms vectors from the inertial frame to the leg frame. Finally, we know that $b_{i,z} = 0$ so that equations (14)-(16) can now be solved for $b_{i,x}$ and $b_{i,y}$.

2.2.2 Velocity and Acceleration Inverse Kinematics

From Figures 2 and 4 we obtain:

$$\dot{\mathbf{q}} + \boldsymbol{\omega}_p \times \mathbf{p}_{abs}^i + \boldsymbol{\omega}_{leg}^i \times l_i \mathbf{z}_{leg}^i = \dot{\mathbf{b}}_i \tag{17}$$

where $\boldsymbol{\omega}_{leg}^i = \boldsymbol{\omega}_p + \dot{\zeta}_i \mathbf{x}_{leg}^i$ is the angular velocity of the leg. Also, from Figures 2 and 4 it can be derived that:

$$\zeta_i = \cos^{-1}\left(\frac{-\mathbf{p}_{abs}^i{}^T \mathbf{r}_i}{l_i \left\|\mathbf{p}_{abs}^i\right\|}\right) = \cos^{-1}\left(\frac{-\mathbf{p}_{abs}^i{}^T \left(\mathbf{b}_i - \mathbf{q} - \mathbf{p}_{abs}^i\right)}{l_i \left\|\mathbf{p}_{abs}^i\right\|}\right) \qquad (18)$$

Equations (17) and (18) can be solved for $\dot{\mathbf{b}}_i$ using the same procedure as in the velocity inverse kinematics of the previous joint configuration (Sec. 2.1), where instead for angle β_i we now have angle ζ_i.

By differentiating equation (17), we obtain:

$$\ddot{\mathbf{q}} + \dot{\boldsymbol{\omega}}_p \times \mathbf{p}_{abs}^i + \boldsymbol{\omega}_p \times \left(\boldsymbol{\omega}_p \times \mathbf{p}_{abs}^i\right) + \ddot{\zeta}_i \times l_i \mathbf{z}_{leg}^i + \dot{\zeta}_i \times l_i \dot{\mathbf{z}}_{leg}^i = \ddot{\mathbf{b}}_i \qquad (19)$$

Now, using the same process as in the previous joint configuration inverse kinematics analysis, vector $\ddot{\mathbf{b}}_i$ can be obtained.

2.3 AGV inverse Kinematics

The model of the AGV is shown in top view in Figure 5. The AGV has three wheels that are driven simultaneously by the same motor. Another motor steers the three wheels simultaneously (Synchro-drive) and so they are always pointing in the same direction. The orientation of the AGV remains constant, while the three wheels turn simultaneously towards the direction of motion. If θ is the driving angle and ψ is the steering angle of the wheels, then from Figure 5 we find that:

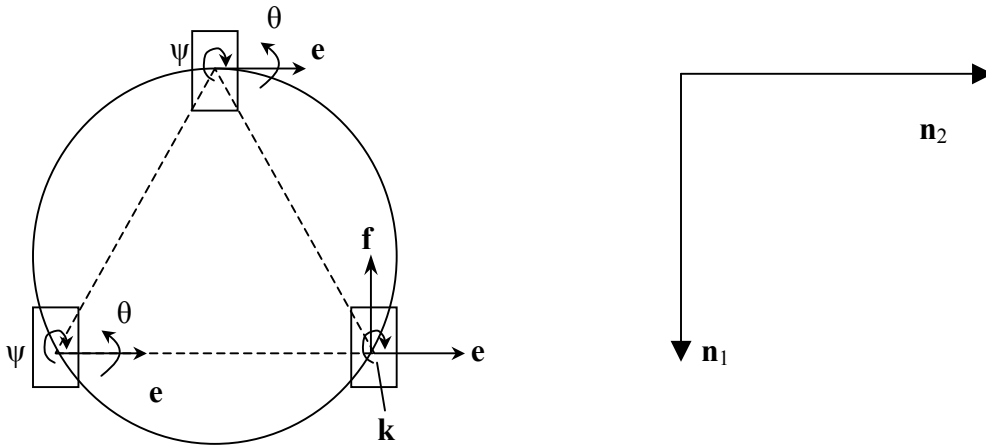$$\psi = \arctan\left(\frac{\dot{b}_{i,x}}{\dot{b}_{i,y}}\right) \qquad (20)$$

Figure 5. Top view of the Synchro-drive AGV. In this figure, $\psi = -\pi/2$.

Also from Figure 5 we can obtain $\dot{\theta}$:

$$\dot{\theta} = \frac{\sqrt{\dot{b}_{i,x}^2 + \dot{b}_{i,y}^2}}{r_{wheel}} \tag{21}$$

where r_{wheel} is the radius of the wheels of the AGV.

By differentiating equation (20), $\dot{\psi}$ can be obtained:

$$\dot{\psi} = \frac{\ddot{b}_{i,y}\dot{b}_{i,x} - \dot{b}_{i,y}\ddot{b}_{i,x}}{\dot{b}_{i,x}^2 + \dot{b}_{i,y}^2} \tag{22}$$

Finally, by differentiating equation (21), $\ddot{\theta}$ is obtained:

$$\ddot{\theta} = \frac{\dot{b}_{i,x}\ddot{b}_{i,x} + \dot{b}_{i,y}\ddot{b}_{i,y}}{r_{wheel}\sqrt{\dot{b}_{i,x}^2 + \dot{b}_{i,y}^2}} \tag{23}$$

The time derivatives $\dot{\mathbf{b}}_i$ and $\ddot{\mathbf{b}}_i$ are known from the platform's velocity and acceleration inverse kinematics solutions. However, if equation (22) is to be differentiated in order to obtain $\ddot{\psi}$, the time derivatives of the accelerations will be needed. To avoid this, $\ddot{\psi}$ is approximated as follows:

$$\ddot{\psi} = \frac{\dot{\psi} - \dot{\psi}_{prev}}{\Delta t} \tag{24}$$

where $\dot{\psi}$ is calculated using equation (22) while $\dot{\psi}_{prev}$ is the value of $\dot{\psi}$ calculated at the previous time step, Δt being the elapsed time between two steps.

3. Inverse Dynamics Analysis

3.1 Platform Inverse Dynamics

Neglecting the leg inertias, it is apparent from Figure 6 that:

$$\sum \mathbf{f}^i = \mathbf{f}_1^i + \mathbf{f}_2^i = \mathbf{0}$$
$$\sum \mathbf{n}^i = \mathbf{n}_1^i + \mathbf{n}_2^i + \mathbf{r}_i \times \mathbf{f}_2^i = \mathbf{0} \tag{25}$$

where $\mathbf{r}_i$ is the vector from the point of application of $\mathbf{f}_1^i$ to the point of application of $\mathbf{f}_2^i$.
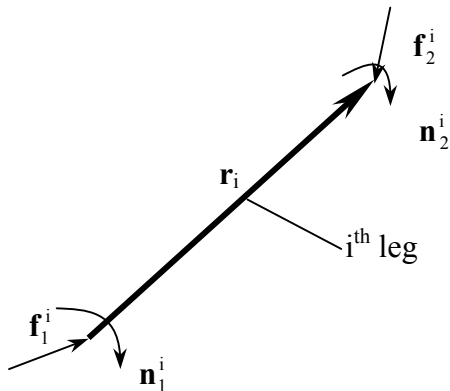

Figure 6. Free body diagram for the ith leg.

Both configurations of the leg considered in this work include a passive revolute joint at one end of the leg. Since this revolute joint cannot support any moment about its axis, we have the additional condition that:

$$\left[\mathbf{r}_i \times \mathbf{R}_i^T \mathbf{f}_2^i\right]_x = 0 \tag{26}$$

where $\mathbf{R}_i$ is the orientation matrix that transforms vectors from the ith leg frame to the inertial frame, and the subscript x indicates the component about the leg's x-axis.

The equations of motion of the platform are:

$$-\mathbf{f}_2^1 - \mathbf{f}_2^2 - \mathbf{f}_2^3 = m\mathbf{a} \tag{27}$$

$$-\mathbf{p}_{abs}^1 \times \mathbf{f}_2^1 - \mathbf{p}_{abs}^2 \times \mathbf{f}_2^2 - \mathbf{p}_{abs}^3 \times \mathbf{f}_2^3 = \mathbf{R}(\mathbf{I}\dot{\boldsymbol{\omega}} + \boldsymbol{\omega} \times \mathbf{I}\boldsymbol{\omega}) \tag{28}$$

where $\mathbf{a}$ is the translational acceleration of the moving platform's mass center, expressed in the inertial frame. The matrix $\mathbf{I}$ is the inertia matrix of the platform (expressed in the platform's body frame), while $\boldsymbol{\omega}$ and $\dot{\boldsymbol{\omega}}$ are the angular velocity and acceleration of the platform, expressed in the body frame. Equations (26), (27) and (28) can be solved for the nine components of the three forces $\mathbf{f}_2^1, \mathbf{f}_2^2$ and $\mathbf{f}_2^3$.

3.2 AGV Inverse Dynamics

For each of the components of the AGV (three wheels and a platform), the following equation can be written:

$$\mathbf{M}_i \dot{\mathbf{t}}_i + \mathbf{W}_i \mathbf{M}_i \mathbf{t}_i = \mathbf{w}_i \tag{29}$$

where i=1,2,3 for the three wheels and i=4 for the platform of the AGV. In equation (29) we have:

$$\mathbf{M}_i = \begin{bmatrix} \mathbf{I}_i & \mathbf{0} \\ \mathbf{0} & m_i \mathbf{I}_{3x3} \end{bmatrix}$$

where $\mathbf{I}_i$ is the inertia matrix of body i, and the twist of the body is given by:

$$\mathbf{t}_i = \begin{bmatrix} \boldsymbol{\omega}_i \\ \dot{\mathbf{c}}_i \end{bmatrix}$$

where $\mathbf{c}_i$ is the position vector of the mass center of i.

$$\mathbf{W}_i = \begin{bmatrix} \boldsymbol{\Omega}_i & \mathbf{0} \\ \mathbf{0} & \mathbf{0} \end{bmatrix}$$

where $\boldsymbol{\Omega}_i$ is the cross-product matrix of $\boldsymbol{\omega}_i$. In addition, $\mathbf{w}_i$ is the wrench vector of body i. Equation (29) can now be assembled for all four parts of the AGV:

$$\mathbf{M}\dot{\mathbf{t}} + \mathbf{WMt} = \mathbf{w} \tag{30}$$

It is important to note that in this equation:

$$\mathbf{t} \equiv \begin{bmatrix} \mathbf{t}_1 \\ \mathbf{t}_2 \\ \mathbf{t}_3 \\ \mathbf{t}_4 \end{bmatrix} = \begin{bmatrix} \mathbf{e} & \mathbf{k} \\ -\mathbf{r}_{\text{wheel}}\mathbf{f} & 0 \\ \mathbf{e} & \mathbf{k} \\ -\mathbf{r}_{\text{wheel}}\mathbf{f} & 0 \\ \mathbf{e} & \mathbf{k} \\ -\mathbf{r}_{\text{wheel}}\mathbf{f} & 0 \\ 0 & 0 \\ -\mathbf{r}_{\text{wheel}}\mathbf{f} & 0 \end{bmatrix} \begin{bmatrix} \dot{\theta} \\ \dot{\psi} \end{bmatrix} = \mathbf{T}\dot{\boldsymbol{\theta}} \tag{31}$$

where the unit vectors $\mathbf{e}$, $\mathbf{f}$ and $\mathbf{k}$ are shown in Figure 5. Pre-multiplying both sides of equation (30) by $\mathbf{T}^{\text{T}}$, we obtain:

$$\mathbf{T}^{\text{T}}\left(\mathbf{M}\dot{\mathbf{t}} + \mathbf{WMt}\right) = \mathbf{T}^{\text{T}}\left(\mathbf{w}^{\text{w}} + \mathbf{w}^{\text{c}}\right) = \mathbf{T}^{\text{T}}\mathbf{w}^{\text{w}} + \mathbf{T}^{\text{T}}\mathbf{w}^{\text{c}} \tag{32}$$

where $\mathbf{w}^{\text{w}}$ and $\mathbf{w}^{\text{c}}$ are the working and the constraint wrench correspondingly. Now, since the power due to constraint wrench is equal to zero, we have:

$$\mathbf{t}^{\text{T}}\mathbf{w}^{\text{c}} = 0 \tag{33}$$

But from equation (31), it can be obtained that:

$$\mathbf{t}^{\text{T}} = \left(\mathbf{T}\dot{\boldsymbol{\theta}}\right)^{\text{T}} = \dot{\boldsymbol{\theta}}^{\text{T}}\mathbf{T}^{\text{T}} \tag{34}$$

Combining equations (33) and (34), we obtain:

$$\dot{\boldsymbol{\theta}}^{\text{T}}\mathbf{T}^{\text{T}}\mathbf{w}^{\text{c}} = 0 \tag{35}$$

If $\dot{\boldsymbol{\theta}}$ is independent then the equation (35) becomes:

$$\mathbf{T}^{\text{T}}\mathbf{w}^{\text{c}} = \mathbf{0} \tag{36}$$

So, from equations (32) and (36), we have:

$$\mathbf{T}^{\text{T}}\left(\mathbf{M}\dot{\mathbf{t}} + \mathbf{WMt}\right) = \mathbf{T}^{\text{T}}\mathbf{w}^{\text{w}} \tag{37}$$

The working wrenches ($\mathbf{w}^{\text{w}}$) can be further split into motor-working wrenches ($\mathbf{w}^{\text{wm}}$) and external wrenches ($\mathbf{w}^{\text{we}}$). Then, the required motor torques are nothing but the vector $\boldsymbol{\tau}_{\text{mot}} = \mathbf{T}^{\text{T}}\mathbf{w}^{\text{wm}}$. So, equation (37) gives:

$$\boldsymbol{\tau}_{\text{mot}} = \mathbf{T}^{\text{T}}\left[\mathbf{M}\dot{\mathbf{t}} + \mathbf{WMt} - \mathbf{w}^{\text{we}}\right] \tag{38}$$

This equation can be solved directly for $\boldsymbol{\tau}_{\text{mot}}$ since all the right-hand side elements are known.

4. Simulations

The platform of the simulated mechanism consists of a cylinder of radius of 0.06 m and thickness 0.01 m, with a mass of 0.8 kg. On the cylinder, the leg attachment points form an equilateral triangle (Figure 1). The length of each leg is 0.2 m.

Two maneuvers were simulated using the mathematical model developed in the preceding sections. Both maneuvers are performed for both joint-configuration mechanisms with the same starting points for the three AGVs.

4.1 First Maneuver

In the first maneuver, the platform undergoes pure translation from t = 1 s to t =3 s along the $\mathbf{n}_1$, $\mathbf{n}_2$ and $\mathbf{n}_3$ axes simultaneously, with sinusoidal acceleration in each direction. The total displacement of the upper platform is 1 m along the $\mathbf{n}_1$ axis, 1 m along the $\mathbf{n}_2$ axis and 0.04 m along the $\mathbf{n}_3$ axis. The resulting AGV trajectories for this maneuver are shown in Figure 7. Note that in Figure 7 the further apart the dots of the dotted lines are, the faster the AGV is moving (a result of the non-constant acceleration).

One important observation for this maneuver is that the two joint configurations have the same behavior for pure translation movements of the platform and thus all their plots were identical.

As a result of the changing height of the upper platform, the leg angle β_i changes from 48.6° at the start of the maneuver to 71.8° at the end of the maneuver. It should be noted that the horizontal translation in this maneuver is very large relative to the size of the mechanism, thus illustrating the large workspace of this mechanism in this direction.

The forces exerted by the legs on the AGVs are shown in Figure 8, while the required friction ($\mu = \dfrac{\sqrt{f_x^2 + f_y^2}}{f_z}$) for the three AGVs is shown in Figure 9. The required friction coefficient is found to be relatively large, changing from about 0.9 at the start of the maneuver to 0.3 at the end of the maneuver. Assuming that it would be unreasonable to expect a friction coefficient larger than 1.0, this implies that the value of β_i should not go under 45° during the operation of this mechanism.

The required motor torques for the three AGVs are also shown in Figure 9. It is noted that the required motor torques are not zero for the driving motors, even when the AGVs are not moving. This is so because even then, a torque is required just to keep the AGV stationary. As well, we note that the steering torques are extremely small for all three wheels.
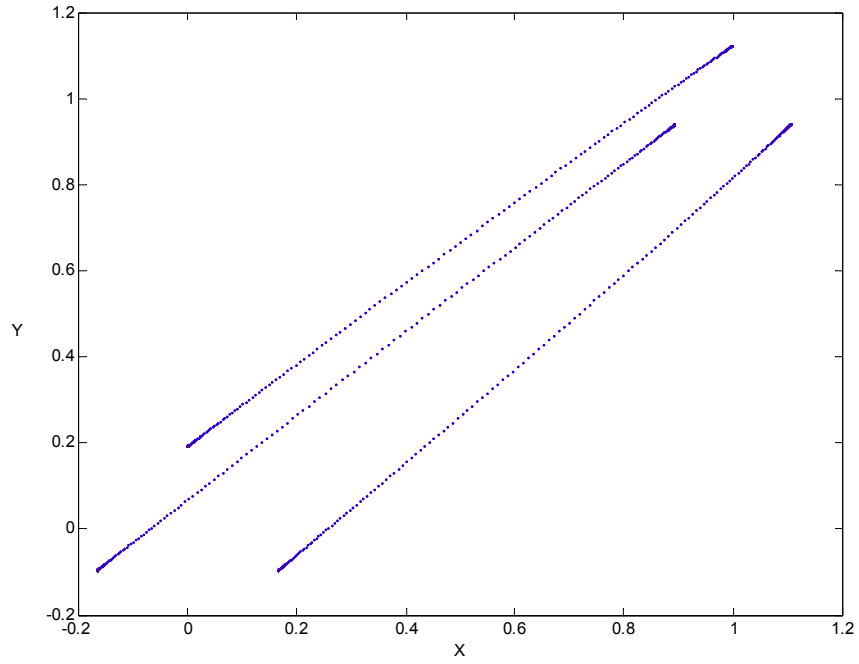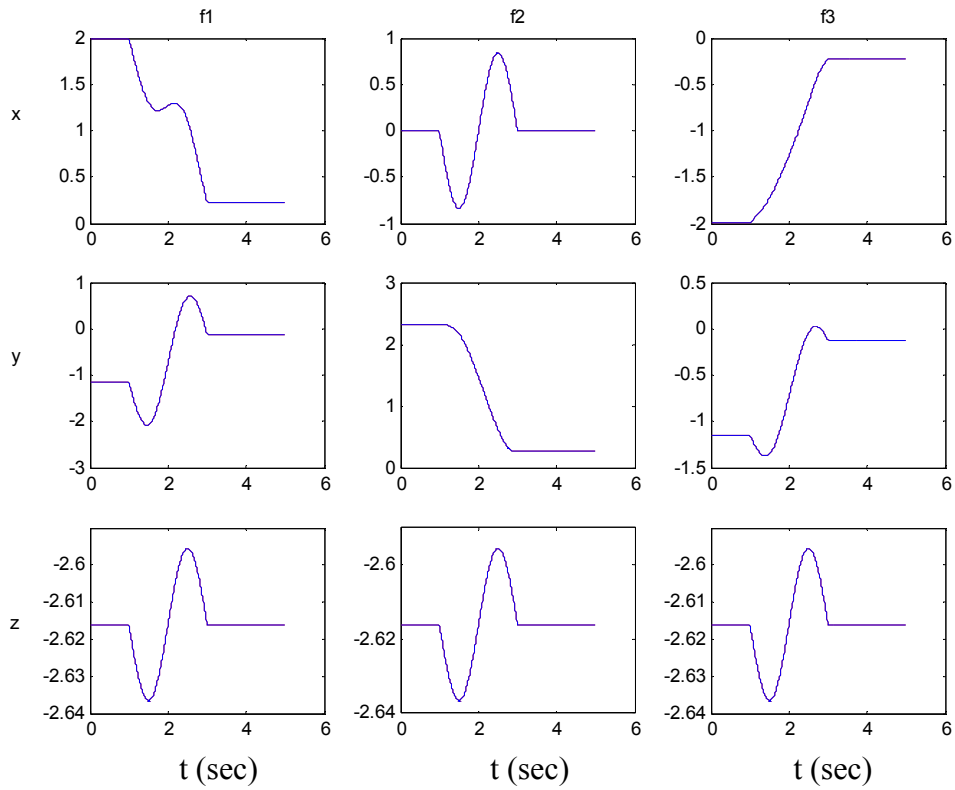
Figure 7. Movement of the AGVs for the first maneuver.

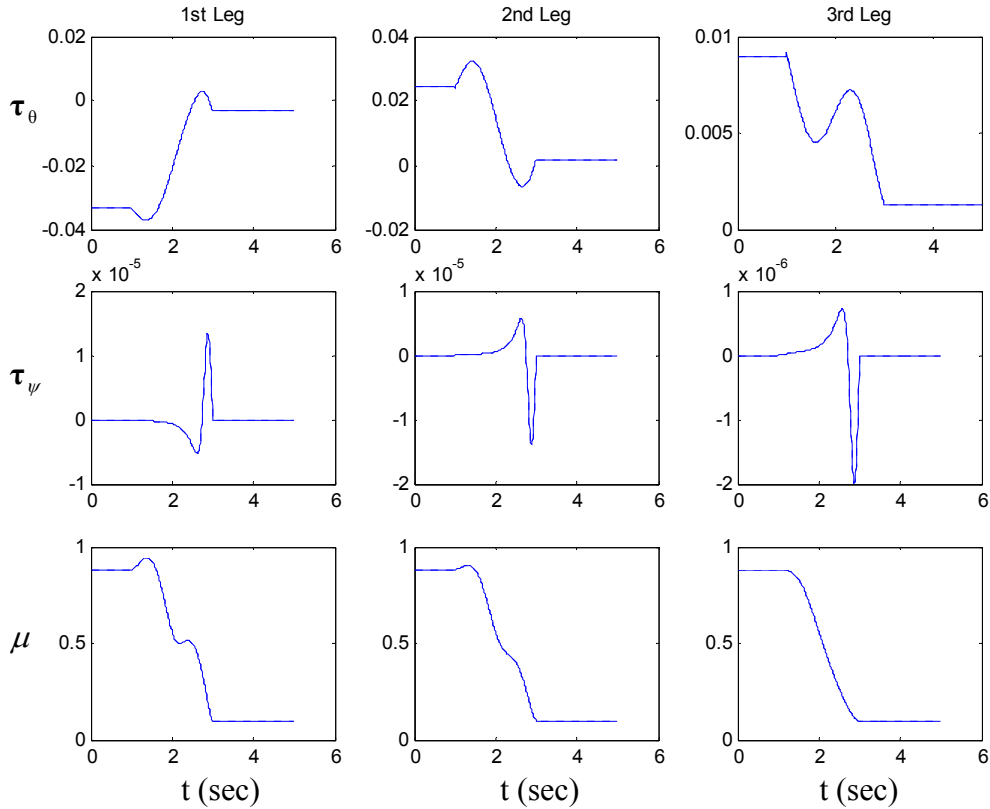**Figure 8.** x-y-z components of the forces applied by each of the three legs to the AGVs

Figure 9. Required motor torques (τ_θ and τ_ψ) and friction coefficient (μ) for the three AGVs for the first maneuver.

4.2 Second Maneuver

In the second maneuver, the platform undergoes a pure rotation of 22.9° from t = 1 s to t = 3 s about the $\mathbf{n}_3$ axis, with sinusoidal acceleration. The resulting trajectories for this maneuver are shown in Figure 10. Since the height of the upper platform stays constant, the leg angle β_i remains at its initial value of 48.6° throughout the maneuver.

In this maneuver, the two configurations behave differently. In Figures 10, 11 and 12 the dashed lines correspond to the configuration with the ball joints at the AGVs and the revolute joints at the platform. From Figure 10, we observe that the configuration with the revolute joints at the AGVs requires far smaller movements of the AGVs, for the same movement of the platform. As a result, more accurate control would be needed for this configuration.

The forces exerted by the legs on the AGVs are shown in Figure 11. In this maneuver, the leg forces are quite similar for the two configurations, and we note that the vertical force stays constant. The required friction for the three AGVs is shown in Figure 12. It is interesting that for the configuration with the spherical joints at the lower end of the legs, the friction coefficient stays constant throughout the maneuver.

The required motor torques for the three AGVs are also shown in Figure 12. Once again, the steering torques remain very small.
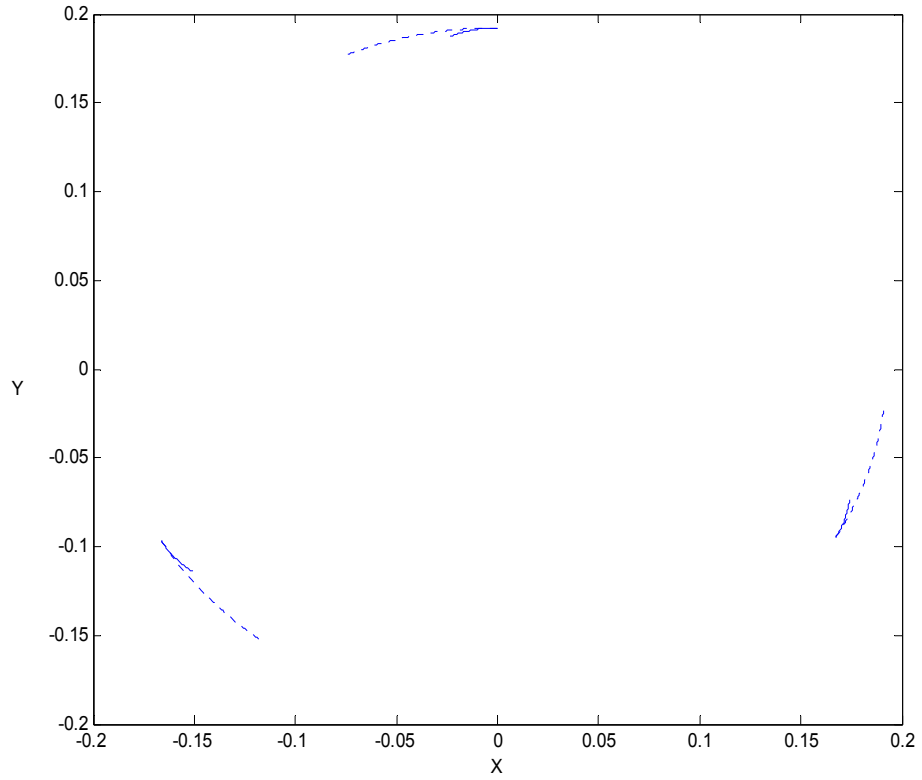
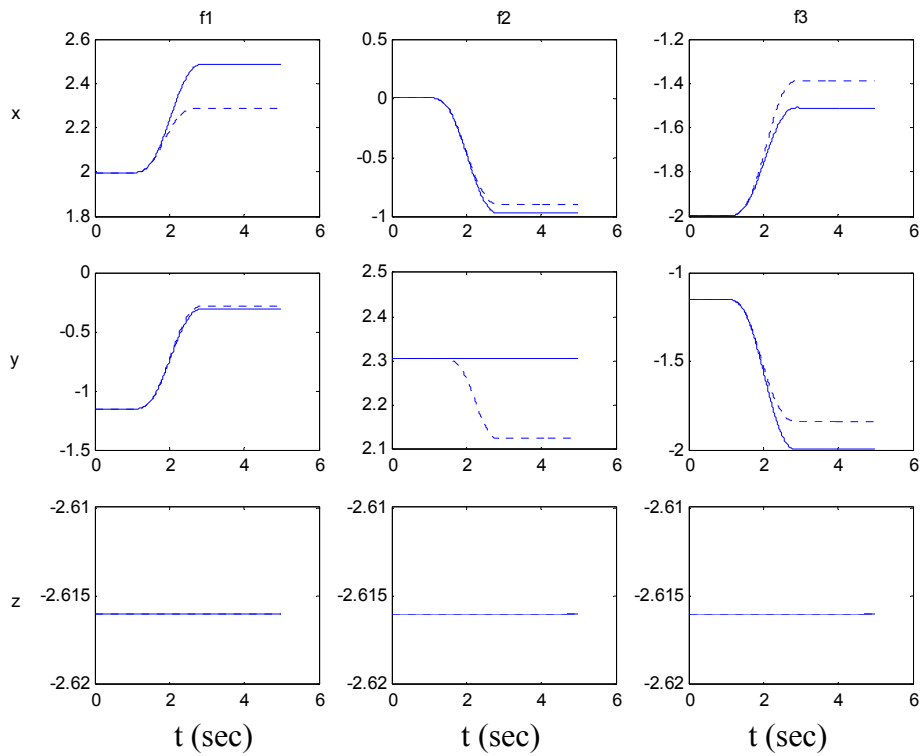**Figure 10.** Movement of the AGVs for the second maneuver.

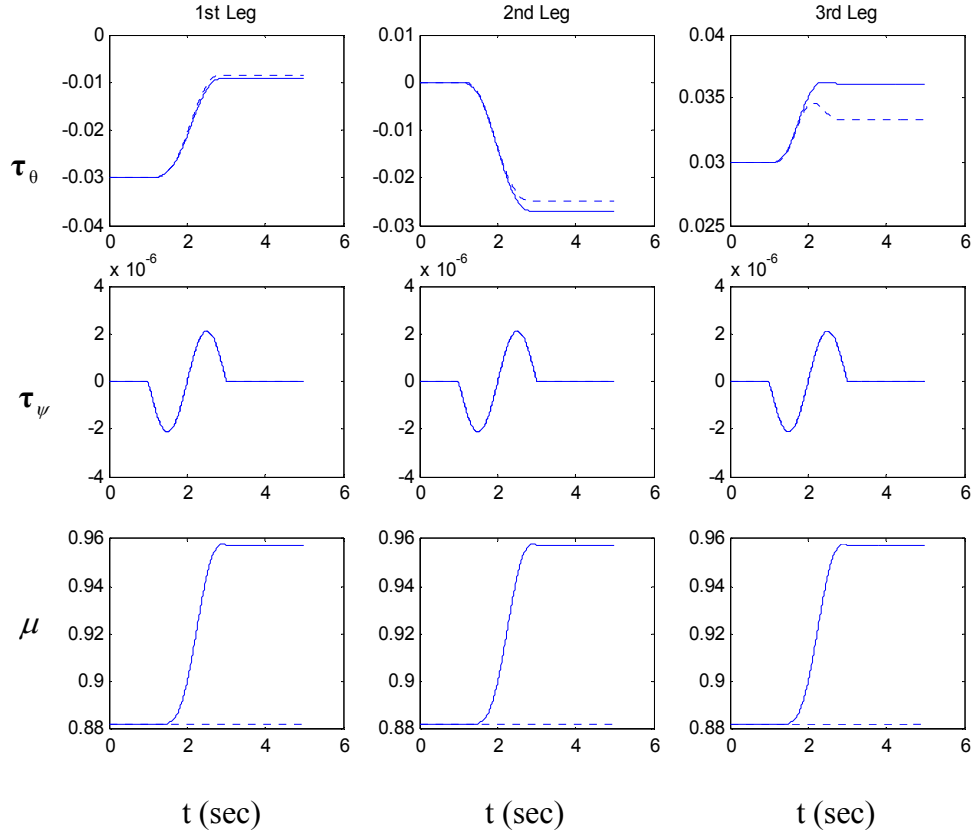**Figure 11.** x-y-z components of the forces applied by the legs to the AGVs.

Figure 12. Required motor torques (τ_θ and τ_ψ) and friction (μ) for the three AGVs for the second maneuver.

5. Conclusions

In this paper, the complete inverse kinematics (position, velocity and acceleration) and dynamics analysis of a 3-legged parallel robotic mechanism with AGV actuators are presented. Two different joint configurations are evaluated. It is shown that when the platform of the mechanism undergoes pure translation, the two configurations behave in the same way. In addition, the friction coefficient required is found to be relatively large, thus restricting the workspace in the vertical direction and the rotational workspace. On the contrary, the workspace in the horizontal direction is restricted only by the availability of the area on which the AGVs are moving. It is also found that the configuration with ball joints at the top of the legs requires very small motion of the AGVs in certain maneuvers, and hence will require more precise control for these motions. Thus, the configuration with the ball joints at the base of the legs is preferred.

References

[1] Gough V. E. "Contribution to discussion to papers on research in automobile stability and control and in tyre performance, by Cornell staff", Proc. Auto. Div. Instn mech. Engrs 1956-57, 392.

[2] Stewart D. "A platform with six degrees of freedom" Proc. Inst. Mech. Engr. (London) 1965;180(1):371-386.

[3] Chen N. X., Song S. M. "Direct Position Analysis of the 4-6 Stewart platforms", ASME Conference on Robotics, Spatial Mechanisms and Mechanical Systems, 1992;DE-45

[4] Innocenti C., Parenti-Castelli V. "A novel numerical approach to the closure of the 6-6 Stewart platform mechanism", Proc. IEEE Int. Conf. On Robotics and Automation, 1991; 851-855.

[5] Lin W., Crane C. D., Duffy J. "Closed-form forward displacement analysis of the 4-5 in-parallel platforms", ASME Conf. On Robotics, Spatial Mechanisms and Mechanical Systems, 1992; DE-45.

[6] Ben-Horin R., Shoham M. "Construction of a six-degree-of-freedom parallel manipulator with three planarly actuated links" Proc. ASME Design Engineering Technical Conferences and Computers in Engineering Conference, 18-22 August 1996.

[7] Ben-Horin R., Shoham M. Djerassi S. "Kinematics, dynamics and construction of a planarly actuated parallel robot" Robotics and Computer-integrated Manufacturing, v.14 (1998) p.163-172.

[8] Tsai L. W., Tahmasebi F. "Synthesis and analysis of a new class of six-degrees-of-freedom parallel minimanipulators". J. Robotic Systems 1993;10(5):561-80.

[9] Tsai L. W., Tahmasebi F. "Closed-form direct kinematics solution of a new parallel minimanipulator". ASME J. Mech. Des. 1994;116:1141-147.

[10] Tahmasebi F., Tsai L. W. "On the stiffness of a novel six-degrees-of-freedom parallel minimanipulator". J. Robotic Systems 1995;12(12):845-56.